ELSEVIER

Journal of Nuclear Materials 313–316 (2003) 852–856

journal of nuclear materials

www.elsevier.com/locate/jnucmat

The relation between edge and divertor plasmas in the Large Helical Device

S. Masuzaki *, N. Ohyabu, T. Morisaki, M. Goto, K. Kawahata, A. Komori, S. Morita, K. Narihara, B.J. Peterson, K. Tanaka, T. Tokuzawa, O. Motojima, LHD Experimental Group

National Institute for Fusion Science, Oroshi 322-6, Toki, Gifu 509-5292, Japan

Abstract

The relation between edge and helical divertor plasmas in the Large Helical Device are presented, in particular electron density n_e and temperature T_e behaviors, by line-averaged density $\bar{n}_e$ scan ($\bar{n}_e \sim 1$–8×10^{19} m^{-3}) in the two typical magnetic configurations with relatively 'thin' and 'thick' naturally stochastic boundaries, respectively. The relations appear to be different in these configurations. With increasing $\bar{n}_e$, detachment-like behaviors of n_e and T_e are observed in the thick stochastic boundary configuration. On the other hand, both n_e and T_e at the divertor plate are almost proportional to them at near the last closed flux surface independent of $\bar{n}_e$. The different characteristics of particle screening and radiation power profile are suggested as causes of the different edge–divertor relations in these stochastic boundaries.

PACS: 52.40.Hf
Keywords: LHD; Divertor; Ergodic boundary; Particle and heat transport; Profile stiffness; Detachment

1. Introduction

One of the characteristics of the heliotron-type magnetic configuration is the existence of the naturally stochastic boundary layer and the intrinsic divertor (helical divertor, HD). In the Large Helical Device (LHD), the largest heliotron-type superconducting device, plasma experiments under the open HD configuration have been performed since 1998 [1]. One of the main issues in this experimental stage is to understand the HD properties in order to design an active particle control system using the HD with appropriate baffles and pumping system. Stochastic boundary layer is also generated with an additional perturbation field in tokamaks, that is, the ergodic divertor configuration (ED) [2]. The expected effect of the ED is a local enhancement of energy and particle transport, leading to the generation of a dense and cold edge region to reduce the sputtering rate, to achieve high pumping efficiency and a strong radiation layer for the reduction of the divertor heat load. Such favorable properties can be expected also in the natural stochastic boundary layer in the LHD. Energy and particle transport in the stochastic boundary are more complicated than the SOL in axisymmetric divertor tokamaks, because of the coexistence of a stochastic region, residual islands and a non-ergodized region (so called 'laminar', in ED devices), and the transport has been investigated theoretically [3] and experimentally [4].

In the LHD, a detailed understanding of the transport in the stochastic boundary ('ergodic layer' in following part) is necessary to realize the effective heat and particle control using the HD, and theoretical and experimental investigations have been conducted. Particle transport was simulated using field line tracing with

* Corresponding author. Tel.: +81-572 58 2145/2168; fax: +81-572 58 2618.
E-mail address: masuzaki@lhd.nifs.ac.jp (S. Masuzaki).

0022-3115/03/$ - see front matter
PII: S0022-3115(02)01461-7

a random walk process to predict the particle deposition profile on the HD. The simulated results were qualitatively consistent with the measured particle deposition using Langmuir probes [5]. The effective radial heat conductivity (χ_e^{eff}) is deduced using the radial profiles of the electron density and temperature in the ergodic layer measured by Thomson scattering, and the relations between the radial profiles of χ_e^{eff} and the Kormogorov length are investigated [6]. In this study, the relation between edge and HD plasmas in the LHD are investigated as a step to a detailed understanding of the energy and particle transport in the ergodic layer.

2. Edge magnetic structure in the LHD

The magnetic structure of the ergodic layer in the LHD [7] is modified depending on the operational magnetic configuration, such as the radial position of the magnetic axis (R_{ax}). In this study, two operational configurations, $R_{ax} = 3.6$ and 3.75 m, are selected for analysis. In the configuration with $R_{ax} = 3.6$ m, better confinement performance is observed, and it is the standard configuration in recent experiment. The configuration has much more favorable particle orbits and mitigates the neoclassical helical ripple transport, while the interchange instability is a concern. On the other hand, in the configuration with $R_{ax} = 3.75$ m, the MHD stability is more optimized [8]. From the point of view of this study, one of the important differences between these two configurations is the volume of the ergodic layer. Fig. 1 shows the profiles of the connection length of field lines (L_c) calculated using field line tracing for these configurations showing the field line structure in the ergodic layer. The starting points of the field line tracing are distributed from the edge of the confinement region to near vacuum vessel along the major radius in the horizontally elongated cross-section. The positions of the last closed flux surface (LCFS) indicate that the volume of the confinement region is larger in the $R_{ax} = 3.6$ m configuration than in the $R_{ax} = 3.75$ m configuration, while the volume of the ergodic layer is larger in the latter case. In the vicinity of the LCFS, L_c is very long ($\gtrsim 1$ km) compared with that in the SOL of axisymmetric divertor tokamaks ($\lesssim 100$ m even in the ITER). Short field lines do not approach the LCFS. The magnetic structure in the divertor is also complicated and three-dimensional reflecting the magnetic structure in the ergodic layer. Field line tracing with a random walk process simulates the particle deposition profile on the HD, and shows the strong non-uniformity of the profile. This non-uniform profile changes depending on the operational magnetic configurations. In the configuration with $R_{ax} = 3.6$ m, particles are mainly deposited on the torus inboard side. On the other hand, the deposition is dominant in the top and bottom region for $R_{ax} = 3.75$ m. The simulated particle deposition profiles were qualitatively consistent with the results of the particle flux measurement using Langmuir probe arrays embedded in three divertor tiles located inboard, outboard and at the bottom of the torus [5]. In this paper hereafter, the configuration with $R_{ax} = 3.6$ and 3.75 m are called the thin and thick ergodic layer configuration, respectively for simplification.

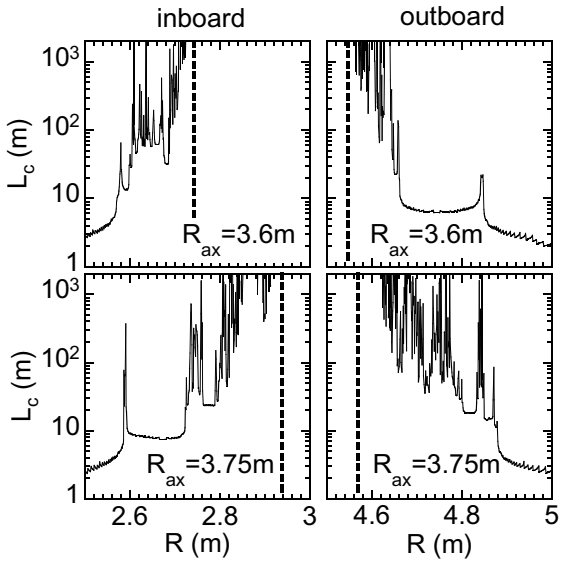

Fig. 1. Calculated magnetic structure of the ergodic layer in the horizontally elongated cross-section in the LHD. The starting points of the field line tracing are distributed on the radial axis at the equatorial plane. The horizontal axis shows the position of the starting points of the field line tracing, and the vertical axis indicates the connection length of the field lines. $R_{ax} = 3.6$ and 3.75 m are the configurations with the thin and the thick ergodic layer, respectively.

3. Experimental

The divertor plasma parameters are measured by the foregoing Langmuir probe arrays. The probe electrodes, 16 ch. per an array, are dome type with 2 mm diameter, and made of isotropic graphite. The distance between electrodes is 6 mm. A single probe method is used for the n_e and T_e measurements. The reference potential is the potential of the vacuum vessel (divertor plates), and a triangular wave of voltage (−210 to +30 V) is applied. The sweep frequency is typically 25 Hz.

T_e at the edge of the confinement region is measured by a Thomson scattering system [9], and the n_e profile is reconstructed from the data of a multi-chord FIR interferometer [10].

The study in this paper is conducted on NBI heated hydrogen discharges fueled with gas puffing, which is the standard operation in the LHD. The toroidal magnetic field strength at the plasma center and the volume averaged beta value deduced from the diamagnetic flux measurement are 2.8 T and <0.65% for the configuration with the thin ergodic layer, 2.64 T and <0.42% for the thick ergodic layer configuration, respectively. In discharges with a relatively higher beta value, typically more than 1%, the magnetic flux surfaces in the edge are destroyed and the magnetic structure of the ergodic layer is modified leading to a change of the particle deposition profile on the divertor [11]. In the discharges analyzed in this study, beta values are low as mentioned above, thus the particle deposition profile is not affected.

4. Results and discussion

Fig. 2 shows n_e and T_e at the edge of the confinement region and at the divertor plate as functions of the line averaged density ($\bar{n}_e$), in the configuration with the thin ergodic layer. The NBI deposition power, P_{dep}, ranges from 4 to 5 MW in these discharges. Due to the three-dimensional structure of the HD, the divertor plasma parameters and their profiles on the divertor plates are strongly depend on the position, such as the toroidal and poloidal angle [5]. In these figures, the divertor plasma parameters shown are measured at the channel at which T_e is the highest of all channels. Long field lines approaching the vicinity of the LCFS are connected to such channels. In Fig. 2(a), both the electron density at the edge of the confinement region ($n_{e,edge}$) and at the divertor plate ($n_{e,div}$) increase with increasing $\bar{n}_e$ up to $\bar{n}_e \sim 8 \times 10^{19}$ m^{-3}. The former is almost proportional to $\bar{n}_e$, and the latter is proportional to $(\bar{n}_e)^{1.45}$. T_e at the edge of the confinement region ($T_{e,edge}$) and at the divertor plate ($T_{e,div}$) are shown in Fig. 2(b) to decrease gradually with the increase in $\bar{n}_e$, and $T_{e,div}$ changes almost linearly with $T_{e,edge}$ ($T_{e,\rho} = 0.97$, where ρ is the normalized minor radius). These results are consistent with the analysis conducted in [5] with lower input power, and there is no sign of the high recycling or the divertor detachment regime observed in tokamaks including those with an ED configuration [12,13]. In the LHD hydrogen plasma, $T_{e,edge}$ is pointed out to be proportional to $(\bar{n}_e)^{-0.5}$ at $\rho = 0.9$ in [14]. Fig. 2(b) is consistent with this scaling. Fig. 2(c) shows the ratios of $T_{e,div}$ and $T_{e,\rho=0.97}$ to $T_{e,\rho=0.97}$ and $T_{e,\rho=0.84}$, respectively. Here, ρ is the normalized minor radius, and $T_{e,\rho=0.97}$ and $T_{e,\rho=0.84}$ indicate the T_e at $\rho = 0.97$ and 0.84, respectively. No clear dependence of both ratios on $\bar{n}_e$ is observed, and it means that the shape of edge T_e profile did not change in this series of discharges. In the LHD, the stiff shape of the T_e profile is observed [14,15], that means, the temperature scale length ($\nabla T_e/T_e$) is preserved nearly independently of the operational conditions, and Fig. 2(c) suggests that the stiff shape of the T_e profile extends to the ergodic layer and, as the result, to the divertor plate.

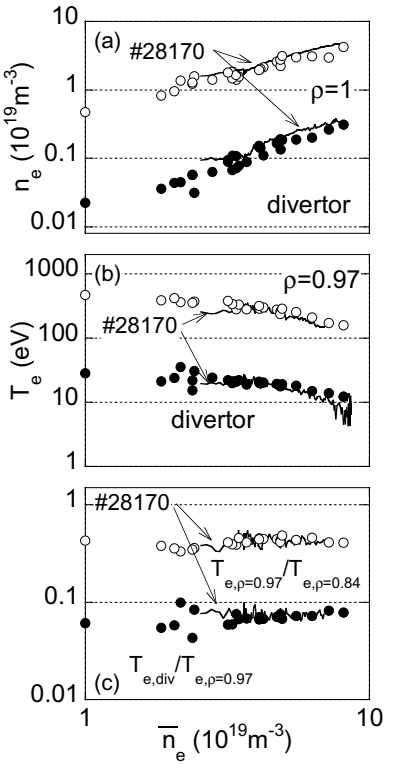

Fig. 2. T_e and n_e in the edge and the divertor plasmas in the configuration with the thin ergodic layer as functions of operational density (line averaged density from the center chord). The NBI power range is 4–5 MW. Open and closed circles are data from different discharges at the timing of the maximum stored energy. Lines shows the time evolution of a discharge (#28170). The normalized minor radius is represented by 'ρ'. (a) Electron density, (b) electron temperature, (c) ratios of electron temperature.

Fig. 3 shows the n_e and T_e data similar to Fig. 2 for the configuration with the thick ergodic layer. The range of P_{dep} and the manner of selecting the Langmuir probe channel are the same as for Fig. 2. In this configuration, $n_{e,div}$ and $T_{e,div}$ behave in different ways from that in the configuration with the thin ergodic layer, and three density regimes are observed (indicated as 'I', 'II', 'III' in Fig. 3). In Fig. 3(a), $n_{e,edge}$ and $n_{e,div}$ are plotted as functions of $\bar{n}_e$, and $n_{e,edge}$ has a similar value to that in the thin ergodic layer case (Fig. 2(a)). With increasing $\bar{n}_e$, $n_{e,div}$ start to decrease at $\bar{n}_e \sim 5.6 \times 10^{19}$ m^{-3} (regime-III). In the low density regime, $T_{e,div}$ and $T_{e,edge}$ are shown in Fig. 3(b) to decrease gradually with increasing $\bar{n}_e$ as observed in the thin ergodic layer configuration, and

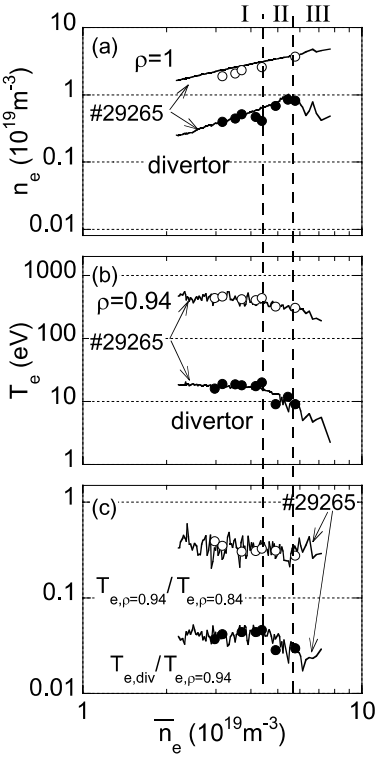

Fig. 3. T_e and n_e in the edge and the divertor plasmas in the configuration with the thick ergodic layer as functions of the operational density. All symbols are the same as Fig. 2. At the top of this figure, I, II, III indicate the density regimes with different divertor plasma characteristics.

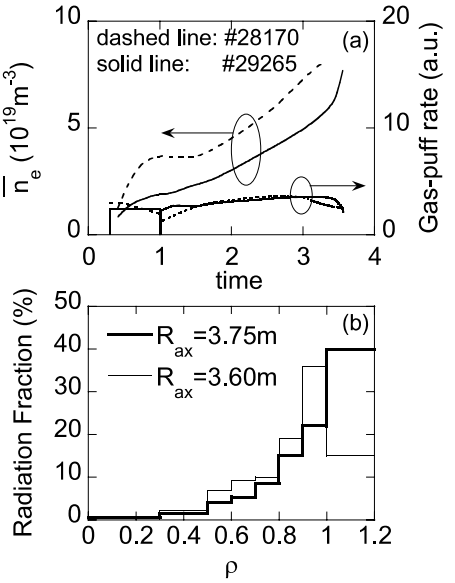

Fig. 4. Characteristic differences between the plasmas in configurations with thin and thick ergodic layers. (a) time evolutions of $\bar{n}_e$ and gas-puff rate (#28170: thin ergodic layer, #29265: thick ergodic layer), (b) profiles of the fraction of radiation power [16] ($R_{ax} = 3.60$ m: thin ergodic layer, $R_{ax} = 3.75$ m: thick ergodic layer).

their density dependences are almost same each other (regime-I). Subsequently, $T_{e,div}$ starts to decrease at $\bar{n}_e \sim 4.5 \times 10^{19}$ m^{-3} independently of $T_{e,edge}$ (regime-II). The behavior of $n_{e,div}$ and $T_{e,div}$ at regime-III is similar to that in the divertor detachment. Fig. 3(c) clearly indicates that the stiffness of the T_e profile shape in the ergodic layer is invalid in the high density regimes (II and III), while it is observed in the lower density regime (I) as in the thin ergodic layer configuration. On the other hand, the stiff shape of the T_e profile is sustained in the edge. In the LHD, regime-III was not stable under the operational condition in this study, and eventually the discharge was terminated by radiative collapse.

As mentioned above, in the configuration with the thick ergodic layer, divertor-detachment-like phenomena are observed, whereas they are not observed in the configuration with the thin ergodic layer. What is the difference between these two configurations? Fig. 4(a) shows the time evolutions of $\bar{n}_e$ and the gas-puffing rate for the discharges with these configurations. The gas puffing rates are shown to be similar, while $\bar{n}_e$ is smaller in the thick ergodic layer case. The larger volume of the ergodic layer in the $R_{ax} = 3.75$ m configuration possibly screens the fueling gas more efficiently than that in the configuration with thin ergodic layer. Thus n_e in the ergodic layer is considered to be higher in the thick case, if the wall condition, such as the wall pumping rate, is the same as in the other discharge. The particle flux to the divertor (Γ_{div}) is amplified due to the screening effect, and $T_{e,div}$ decreases if the power flux to the divertor plate, $q_{div} = \gamma \Gamma_{div} T_{e,div}$ (γ: energy transmission factor in the sheath) is constant. The radiation power profile is also different in these configurations as shown in Fig. 4(b). The profile shape is usually hollow, and the peak position is outside of the LCFS in the thick ergodic layer configuration and at the edge of the confinement region in the thin ergodic layer configuration, respectively. The fraction of the radiation power in the ergodic layer is about 40% for the thick case and about 15% for the other case, typically. There is no clear difference in the total radiation power in these configurations [16]. The difference in fractions of radiation power in the ergodic layer is caused by the difference of the layer's volume. For the higher density and the larger fraction of radiation power in the ergodic layer, it is considered that the high n_e and low T_e divertor plasma is formed in the configuration with a thick ergodic layer in the lower density regime than that in the thin ergodic layer case. In the thin ergodic layer configuration, regime-I is sustained just before the radiative collapse.

5. Summary

The relation between the edge of the confinement region and the divertor plasmas in the magnetic configurations with the thin and the thick stochastic boundary layer are found from the average core density scan ($1–8 \times 10^{19}$ m^{-3}) with an NBI power of 4–5 MW. Three density regimes are recognized in the thick ergodic layer configuration. In the low density range ($\lesssim 4 \times 10^{19}$ m^{-3}), T_e at the divertor plate decreases gradually with density ($\propto \bar{n}_e^{-0.5}$), and is almost proportional to T_e at the LCFS, and that means the shape of the T_e profile is nearly identical from the LCFS to the divertor plate independent of the density (regime-I). T_e at the divertor plate starts to decrease more strongly with increasing density (regime-II). Eventually, the density at the divertor plate also starts to decrease even as the density at the LCFS continues to increase (regime-III). This regime appears to be similar to divertor detachment observed in tokamaks. In the thin ergodic layer configuration, regime-I is sustained over the operational conditions of this study. In the discharges with this configuration, both T_e at the edge of confinement region and $T_{e,div}$ decrease strongly with density just before radiative collapse [5]. The differences in the edge plasma behavior between the regime-III in the thick ergodic layer case and just before the collapse in the thin case suggest that the thick ergodic layer effectively separates the confinement region and the boundary region.

References

[1] A. Iiyoshi et al., Nucl. Fusion 39 (1999) 1245.
[2] Ph. Ghendrih, A. Grosman, H. Capes, Plasma Phys. Control. Fus. 38 (1996) 1653.
[3] A.M. Runov et al., Phys. Plasmas 8 (2001) 916.
[4] Ph. Ghendrih et al., J. Nucl. Mater. 290–293 (2001) 798.
[5] S. Masuzaki et al., Nucl. Fusion 42 (2002) 750.
[6] T. Morisaki et al., these Proceedings.
[7] N. Ohyabu et al., Nucl. Fusion 34 (1994) 387.
[8] H. Yamada et al., Nucl. Fusion 43 (2001) 901.
[9] K. Narihara et al., Phys. Rev. Lett. 87 (2001) 135002.
[10] K. Tanaka et al., J. Plasma Fusion Res. 4 (2002) 427.
[11] S. Masuzaki et al., Plasma Phys. Control. Fus. 44 (2002) 809.
[12] C.S. Pitcher, P.C. Stangeby, Plasma Phys. Control. Fus. 39 (1997) 779.
[13] J. Gunn et al., Plasma Phys. Control. Fus. 41 (1999) B243.
[14] H. Yamada et al., Plasma Phys. Control. Fus. 44 (2002) A245.
[15] N. Ohyabu et al., Plasma Phys. Control. Fus. 44 (2002) A211.
[16] B.J. Peterson et al., J. Nucl. Mater. 290–293 (2001) 930.